Dalton Transactions

ROYAL SOCIETY OF CHEMISTRY

PAPER

View Article Online
View Journal | View Issue

Check for updates

Cite this: *Dalton Trans.*, 2026, **55**, 4813

Formation and tuning of a pillar porous-layered framework into a pillar double-channelled framework

Shuang Liu,[a] Chunze Yu,[b] Sidan Geng[b] and Jingui Duan *[b,c]

Precise structural regulation is crucial for tailoring the functions of metal–organic frameworks (MOFs). In this work, we report a subtle pillar-engineering strategy, which involves changing the hexafluoride anion from SiF_6^{2-} to TiF_6^{2-}, which can trigger a dramatic topological transformation in Cu-based MOFs constructed from 1,3,5-tris(2-methyl-1*H*-imidazol-1-yl)benzene (TMBIB). The resulting frameworks, Cu-TMBIB-a and Cu-TMBIB-b, exhibit entirely different network architectures: Cu-TMBIB-a adopts a classical pillar porous-layered structure with a 3,4,5-c topology, whereas Cu-TMBIB-b features a rare pillar-double-channelled framework with an 8,12-c topology. This distinct evolution in the framework architecture is hierarchically driven by the geometric and electronic disparities between the inorganic pillars, which regulate metal-node coordination and the subsequent assembly process. Notably, Cu-TMBIB-a shows good stability and favorable iodine adsorption performance. This work not only reveals pillar engineering as a powerful tool for MOF topology, but also expands the structural diversity of pillared frameworks, offering a rational design strategy for developing advanced separation materials.

Received 9th January 2026,
Accepted 15th February 2026

DOI: 10.1039/d6dt00054a

rsc.li/dalton

Published on 18 February 2026. Downloaded on 6/17/2026 10:56:24 PM.

1 Introduction

Metal–organic frameworks (MOFs), a class of crystalline porous materials, are constructed by the self-assembly of metal ions or clusters (serving as secondary building units, SBUs) and organic ligands *via* coordinative bonds.[1] Distinguished by their unique structural merits, MOFs feature ultrahigh specific surface areas, tailorable pore dimensions and topological architectures. Additionally, their modular synthesis allows for precise functionalization of frameworks to integrate diverse active sites. These characteristics have rendered MOFs versatile across multiple fields: high-performance proton conductors for anhydrous proton-exchange membrane fuel cells,[2] efficient adsorbents for capturing radioactive iodine from aqueous systems,[3] and promising platforms for gas separation,[4] fluorescence sensing[5] and heterogeneous catalysis.[6] Current research trends for MOFs are moving toward rational structural design for multifunction integration, enhancement of stability under practical working conditions and realization of scalable fabrication,[7] which are expected to address key challenges in energy[8,9] and environmental fields[10–12] and promote their practical deployment.

Building on their tailorable pore dimensions, topological versatility and modular synthesis highlighted above, the incorporation of hexafluoride anions as inorganic pillars has emerged as a pivotal strategy for constructing pillar-layered MOFs, attributed to their robust electrostatic interactions, tunable coordination behaviors and superior structural stability.[13–16] The development trajectory of hexafluoride-based pillar-layered MOFs traces back to pioneering reports on the SIFSIX series, where SiF_6^{2-} pillars bridged 2D metal–organic layers to form 3D frameworks with a **pcu** topology, establishing a fundamental platform for pore size optimization and functionality integration;[17–19] subsequent advancements expanded the repertoire of hexafluoride pillars to PF_6^-, TiF_6^{2-}, GeF_6^{2-} and $NbOF_5^{2-}$, whose distinct bond lengths, ionic radii and electronegativities enabled fine-tuning of interlayer distances and pore microenvironments at the sub-nanometer scale.[20–23] Synthesis regulation has been instrumental in driving structural diversification: ligand design evolved from bidentate linkers (*e.g.*, bipyridine) to multidentate N-containing ligands (*e.g.*, tri(pyridin-4-yl)amine (TPA)[24] and 1,2,4,5-tetra(4-pyridyl) benzene (TPB)),[25] which effectively suppressed framework interpenetration and yielded diverse topologies (*e.g.*, ith-d and fsc) featuring cage-like or hierarchical channel structures, while metal ion substitution (*e.g.*, Zn^{2+} to Cu^{2+}) further modulated coordination geometries to expand pore cavities and opti-

[a]*Henan Engineering Research Center for Green Synthesis of Pharmaceuticals, School of Chemistry & Chemical Engineering, Shangqiu Normal University, Shangqiu 476000, China*
[b]*State Key Laboratory of Chemistry and Utilization of Carbon-Based Energy Resources, College of Chemistry, Xinjiang University, Urumqi, 830000, China. E-mail: duanjingui@xju.edu.cn*
[c]*Nanjing Tech University Suzhou Future Membrane Technology Innovation Center, Suzhou 215300, China*

Published on 18 February 2026. Downloaded on 6/17/2026 10:56:24 PM.

mize host–guest interactions.[26] Notably, subtle variations in pillar identity can alter the pore aperture and channel configuration even under analogous synthetic conditions.[27,28] The intrinsic geometric and electronic disparities between hexafluoride anions themselves constitute a critical regulatory handle, which highlights the potential for precise structural engineering.

Along with our prior explorations in hexafluoride-based pillar-layered MOFs, in which pillar identity, ligand architecture and metal ion selection have been validated as effective levers for structural tuning,[27,28] in the present work, we employed 1,3,5-tris(2-methyl-1*H*-imidazol-1-yl)benzene (TMBIB, Scheme 1) as the organic linker, a rigid tridentate imidazole-containing ligand that can form stable coordination networks. Under liquid–liquid diffusion conditions with analogous temperature, solvent composition and reactant molar ratios, we introduced SiF_6^{2-} and TiF_6^{2-} as inorganic pillars respectively. This approach has led to the formation of two distinct MOF architectures: Cu-TMBIB-a possesses a classic pillar-layered framework, while Cu-TMBIB-b exhibits a unique pillar double-channelled topology. This structural divergence is driven solely by the geometric and electronic differences between the two hexafluoride pillars. This demonstrates the remarkable sensitivity of the framework assembly to subtle variations in inorganic building blocks and achieves promising topological modulation. Notably, Cu-TMBIB-a exhibits exceptional iodine adsorption performance, which underscores the potential of these topology-tailored MOFs as practical adsorbents for iodine-related separation and storage scenarios.

2 Experimental

2.1 Synthesis of the ligand

The organic ligand TMBIB was synthesized *via* a slightly modified solid-state Ullmann reaction as previously reported,[29] using 1,3,5-tribromobenzene and 2-methylimidazole as the starting materials. The chemical structure of TMBIB was confirmed by ^{1}H NMR spectroscopy (400 MHz, $CDCl_3$): δ = 2.498 (s, 9H), 7.091 (d, 3H), 7.102 (d, 3H), 7.351 (s, 3H).

2.2 Synthesis of materials

Both target MOFs were prepared by the liquid–liquid diffusion method. Briefly, metal salts and TMBIB were separately dissolved in different solvents, then sequentially layered in a reaction tube with a solvent buffer layer inserted to slow down the reactant contact rate and facilitate crystallization. The two MOFs share the same TMBIB ligand but differ in their metal salt and inorganic pillar precursor combinations: Cu-TMBIB-a was synthesized using $Cu(OAc)_2$ and $(NH_4)_2SiF_6$, while for Cu-TMBIB-b $CuCl_2$ and $(NH_4)_2TiF_6$ were employed. Detailed synthetic procedures are provided in the SI.

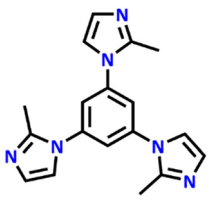

Scheme 1 Ligand TMBIB: (2-methyl-1*H*-imidazol-1-yl)benzene.

3 Results and discussion

3.1 Structure of Cu-TMBIB-a

Cu-TMBIB-a crystallizes in the tetragonal *I*4/*mcm* space group with a formula of $[C_{72}H_{74}Cu_3F_6N_{24}OSi{\cdot}2(SiF_6)]{\cdot}x$Solvent (Table S1). The asymmetric unit of Cu-TMBIB-a consists of two distinct Cu clusters (Cu1 and Cu2), TMBIB ligands, and SiF_6^{2-} inorganic pillars (Fig. S3). Cu1 adopts a 4-c square planar coordination geometry, chelating with four N atoms from different TMBIB ligands, whereas Cu2 functions as a 5-c node with a distorted square pyramidal configuration, coordinated by four ligand N atoms and one lattice O atom. As a rigid tridentate linker, each TMBIB ligand bridges three Cu nodes through its imidazole N atoms, establishing a robust connection between metal centers. The SiF_6^{2-} anions, serving as inorganic pillars, provide structural support for the overall framework. Framework assembly of Cu-TMBIB-a is centered on the formation and connection of SBUs. Cu1 and Cu2 clusters and TMBIB ligands first construct two types of characteristic cage-like SBUs: octahedral cage A and pentahedral cage B. Cage A is composed of two Cu1 clusters, four Cu2 clusters and eight TMBIB ligands (Fig. S4), while cage B comprises four Cu1 clusters, one Cu2 cluster and four ligands (Fig. S5). These two cages are periodically linked by sharing Cu nodes to form a 2D porous layered structure (Fig. 1c). Adjacent 2D layers are vertically supported by SiF_6^{2-} pillars, resulting in a classic pillar-layered 3D framework with an AB-type stacking mode (Fig. 1d) and an interlayer distance of ~6.4 Å, which ensures structural stability and pore connectivity. Connolly surface analysis[30] (probe radius = 1.2 Å) was employed to characterize the porous architecture of Cu-TMBIB-a, revealing two interconnected pore systems within the 3D framework (Fig. 2). Along the *a*-axis, the pores exhibit regular hexagonal cross-sections with pore sizes of ~2.7–2.8 Å, while one-dimensional through-pores are formed along the *c*-axis, matching the internal space of the cage-like SBUs. The calculated solvent-accessible pore volume is substantial, providing ample space for the adsorption and transport of guest molecules, which lays a structural foundation for its excellent iodine adsorption performance. Topological simplification analysis was performed to clarify the framework connectivity:[31] TMBIB ligands are treated as 3-c nodes, SiF_6^{2-} pillars as 2-c nodes, and Cu1/Cu2 clusters as 4-c and 5-c nodes (Fig. 3). This simplification reveals a 3,4,5-c topology, where the connection between nodes adheres to the minimum ring principle, forming a thermodynamically stable network that verifies the rationality of the framework structure.

 This journal is © The Royal Society of Chemistry 2026

Published on 18 February 2026. Downloaded on 6/17/2026 10:56:24 PM.

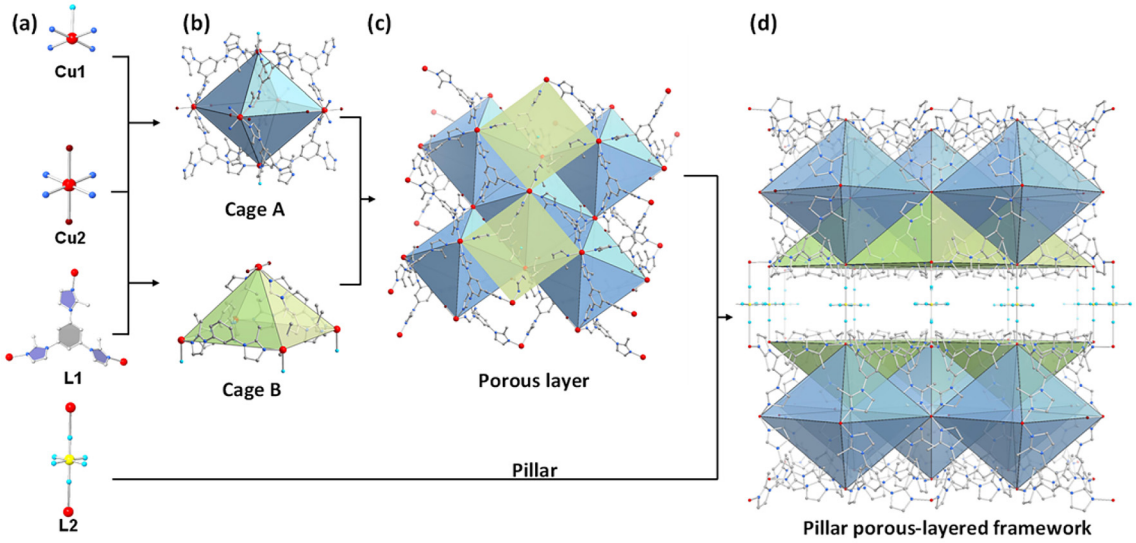

Fig. 1 View of the construction of Cu-TMBIB-a: (a) two kinds of Cu clusters, the connection of ligand TMBIB and SiF_6^{2-}; (b) structures of octahedron cage A and pentahedron cage B, connected by the Cu1 cluster, Cu2 cluster and ligand; (c) the porous layer formed by the former polyhedrons; and (d) the pillar porous-layered framework Cu-TMBIB-a. Cu – red atoms, N – blue, C – gray; hydrogen atoms and the minor disorder components of the ligands.

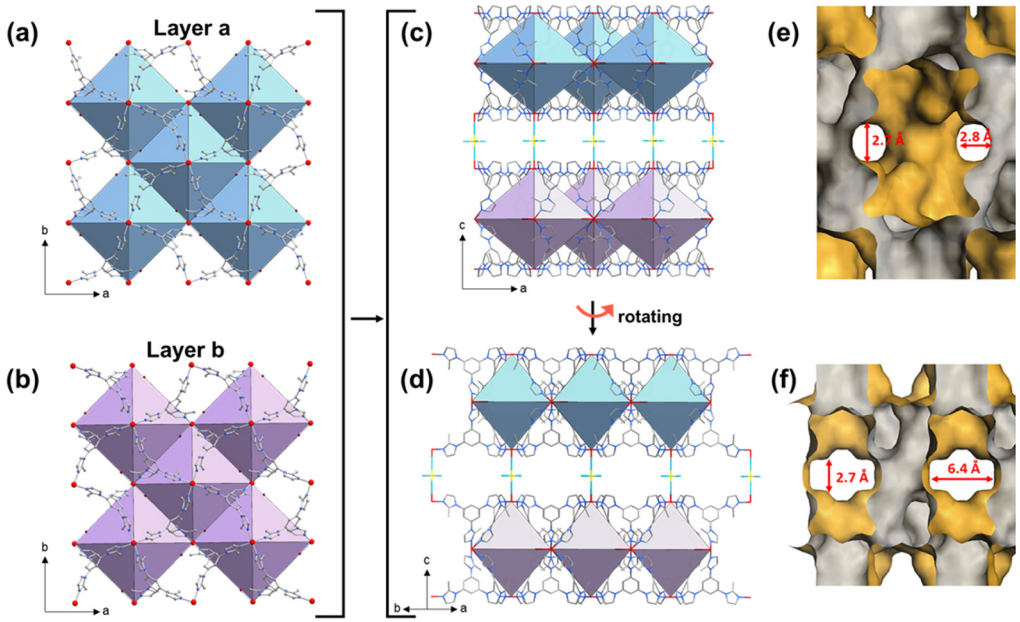

Fig. 2 Views of the structures and accessible pores of Cu-TMBIB-a: (a and b) arrangement of the adjacent layers; (c and d) views of the frameworks along the different directions; and (e and f) the Connolly surfaces display two pore spaces which correspond to (c) and (d), respectively; the radius of the probe is 1.2 Å.

3.2 Structure of Cu-TMBIB-b

Cu-TMBIB-b belongs to the tetragonal *P*4/*mnc* space group with an empirical formula of $[C_{216}H_{216}Cu_{10}F_{30}N_{72}Ti_5]\cdot x$Solvent. Distinct from Cu-TMBIB-a, the asymmetric unit of Cu-TMBIB-b contains three types of Cu nodes (Cu1, Cu2, and Cu3), TMBIB ligands and TiF_6^{2-} inorganic pillars (Fig. S10). Cu1, Cu2 and Cu3 adopt 3-c, 4-c and 5-c coordination modes, respectively, forming diverse coordination geometries through bonding with imidazole N atoms of TMBIB ligands. Notably, the coordination environment of Cu3 is significantly distorted due to the steric hindrance and electronic effects of TiF_6^{2-}. TMBIB ligands retain their tridentate bridging feature but exhibit different coordination angles compared to those in Cu-

Published on 18 February 2026. Downloaded on 6/17/2026 10:56:24 PM.

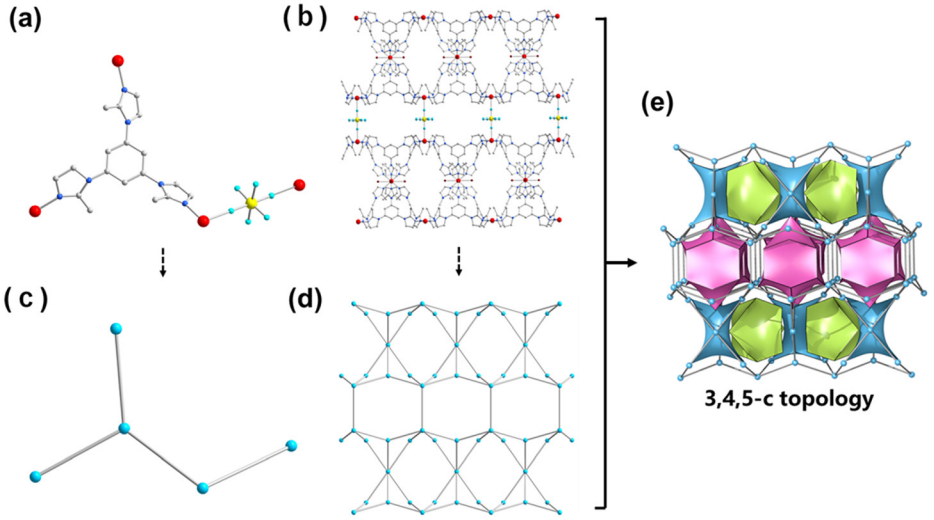

Fig. 3 Schematic representation of the topology of Cu-TMBIB-a: the ligand can be considered as a 3-c node, and SiF_6^{2-} can be considered as a 2-c node.

TMBIB-a, a variation attributed to the geometric and electronic differences between TiF_6^{2-} and SiF_6^{2-}. TiF_6^{2-} anions act as pillars and further stabilize the framework through hydrogen bonding interactions between their F atoms and H atoms on the ligands (Table S3). The framework assembly of Cu-TMBIB-b gives rise to a pillar double-channelled architecture, whose hierarchical structure is comprehensively revealed by structural analysis and pore characterization. Three types of Cu nodes and TMBIB ligands first construct "core–shell" nested layers: the inner layer consists of tetragonal prism channels with an internal pore size of ~20.0 Å, while the outer layer forms approximate cylindrical channels with a larger diameter of ~39.1 Å. These inner and outer layers are covalently linked through shared Cu nodes and ligand segments, ensuring structural cohesion while creating a dual-channel framework. TiF_6^{2-} pillars vertically penetrate the interlayer spaces between adjacent nested layers, transforming into a 3D framework with parallel-stacked double layers and an interconnected channel network (Fig. 4). Complementing this primary dual-channel structure, interstitial pores (~5.2 Å) arise from the geometric mismatch between the inner tetragonal prisms and outer cylinders, acting as "transport corridors" that bridge the inner and outer channels (Fig. 5). Connolly surface analysis[30] further confirms the integrated nature of the pore system: the inner channels (N-rich surfaces) and outer channels (F-enriched surfaces) exhibit heterogeneous surface chemistry, while their seamless connection with interstitial pores yields a hierarchical porous architecture with a significantly total accessible surface area. Topological simplification clarifies the connectivity of this interesting framework: the molecular unit of triangular prisms between the inner and outer channels is defined as a 12-c node, while the ligand groups linking adjacent molecular units function as 8-c nodes (Fig. 6). These nodes are orderly connected *via* coordination bonds to form an 8,12-c topology, an unusual motif among hexafluoride-pillared MOFs that underscores the profound role of inorganic pillar regulation in broadening topological diversity. The phase purity and high crystallinity of the two MOFs were confirmed by PXRD (Fig. S14). In addition, these frameworks start to decompose around 200 °C (Fig. S16).

3.3 Structural evolution and regulation

Cu-TMBIB-a and Cu-TMBIB-b were synthesized using identical reaction parameters *via* the liquid–liquid diffusion method, using TMBIB as the organic linker. The fundamental structural difference between the two MOFs originates solely from the variation of inorganic pillar anions and the corresponding adjustment of metal salts. SiF_6^{2-} features a smaller ionic radius (~2.6 Å) and a symmetric regular octahedral configuration, while TiF_6^{2-} has a larger ionic radius (~2.8 Å) and an uneven electron distribution due to the high electronegativity of Ti^{4+}. These intrinsic differences in geometric and electronic properties directly modulate the coordination modes of metal nodes,[32,33] the conformation of organic ligands[16,34] and the final framework assembly pathway, serving as the core structural switch for the topological transformation. The high symmetry and weak coordination activity of SiF_6^{2-} induce Cu nodes to form two stable coordination modes (4-c and 5-c), while the steric hindrance and electronic effects of TiF_6^{2-} trigger the formation of three coordination configurations (3-c, 4-c and 5-c) for Cu nodes, laying the foundation for structural diversification. Differences in coordination modes further lead to variations in the composition of cage-like SBUs. Cu-TMBIB-a forms octahedral/pentahedral dual-cage structures, while Cu-TMBIB-b constructs triangular prism/tetragonal prism nested interlayer cavities, which directly affect the construction mode of layered structures. The disparity in layered structures ultimately results in a fundamental change in 3D topology, transforming from a classic pillar-layered topology of Cu-TMBIB-a into a unique pillar-double-channelled topology of Cu-TMBIB-

 This journal is © The Royal Society of Chemistry 2026

Published on 18 February 2026. Downloaded on 6/17/2026 10:56:24 PM.

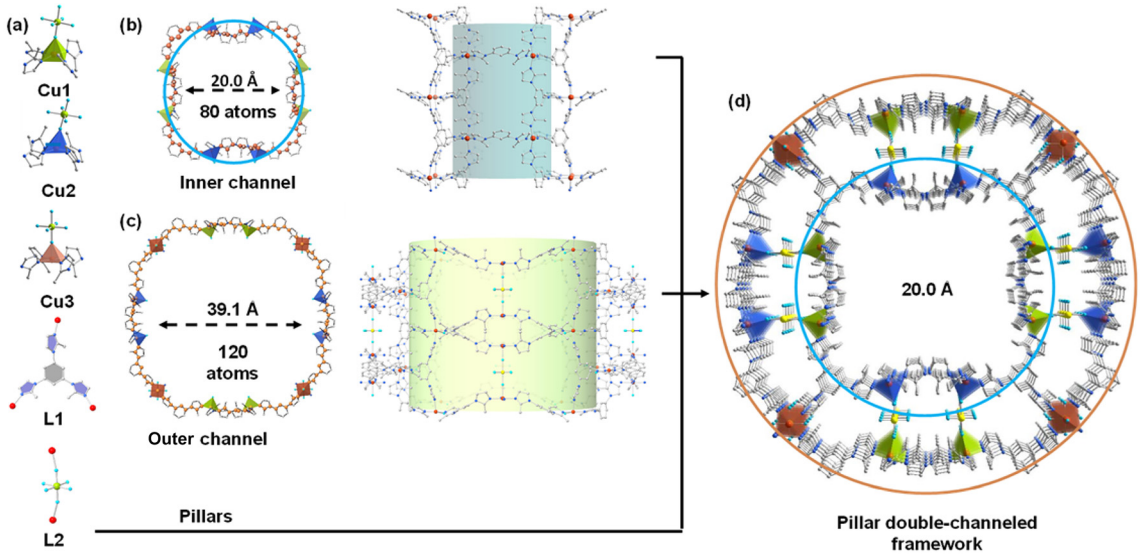

Fig. 4 View of the structure of Cu-TMBIB-b: (a) the coordination modes of three Cu atoms, ligand TMBIB and TiF_6^{2-}; (b and c) views of the inner and outer channels along the different directions; and (d) view of the whole pillar porous-layered framework along the *c*-axis. Cu: red atoms; N: blue; and C: gray; green, blue and brown polyhedra represent the three formed Cu clusters, respectively. Hydrogen atoms and the minor disorder components of the ligands are omitted.

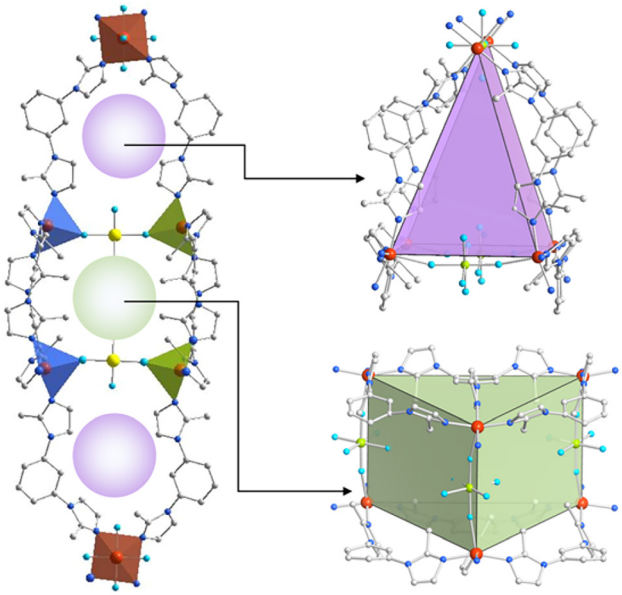

Fig. 5 View of the building block of Cu-TMBIB-b: structure of triangular prism and tetragonal prism cavities between the inner and outer channels.

b. This sequential regulation from the coordination environment to SBUs and finally to the topology realizes the precise design of framework structures through a single variable.

3.4 Iodine adsorption performance of Cu-TMBIB-a

Iodine capture is crucial for industrial processes and environmental remediation. Due to the poor stability of Cu-TMBIB-b, only Cu-TMBIB-a was subjected to systematic iodine adsorption–desorption investigations. XPS quantitative analysis (Table S4) confirmed successful iodine capture, with characteristic I 3d peaks at 618.3 eV (I $3d_{5/2}$) and 629.9 eV (I $3d_{3/2}$) (Fig. 7a). The adsorption capacity was determined to be ~250 mg g^{-1}, comparable to state-of-the-art MOF adsorbents.[3] The PXRD patterns of Cu-TMBIB-a before adsorption, after adsorption, and after desorption all match the simulated pattern, confirming the framework's crystallinity and structural integrity throughout the entire adsorption–desorption cycle. This stability stems from the robust SiF_6^{2-}-pillared architecture and the regular dual-pore system (2.7–2.8 Å and *c*-axis through-pores), which offer ample adsorption sites and space. Desorption experiments evaluated recyclability. The process was monitored *via* UV-Vis spectrophotometry at 5-minute intervals by tracking the characteristic iodine peak at 290 nm (Fig. 7c). To verify equilibrium attainment, monitoring was initially conducted for 90 minutes. The desorption profile showed an initial rapid release (0–30 min), followed by a progressively slowing rate (30–60 min). After 60 minutes, spectral changes became negligible, with absorbance differences between consecutive points below 0.005. A calibration curve (Fig. S18) determined the desorption efficiency at 60 minutes to be ~90%. This timeframe was selected as the optimal endpoint, balancing high desorption performance with practical time considerations for adsorbent recyclability. This favorable reversibility stems from interconnected pore channels that reduce mass transfer resistance and weak framework–iodine interactions, facilitating efficient iodine diffusion without structural damage. The I 3d spectrum of I_2@Cu-TMBIB-a (Fig. 7a) exhibited peaks corresponding to neutral I_2 molecules (618.3 eV, 629.9 eV) with no polyiodide ion signals, indicating

Published on 18 February 2026. Downloaded on 6/17/2026 10:56:24 PM.

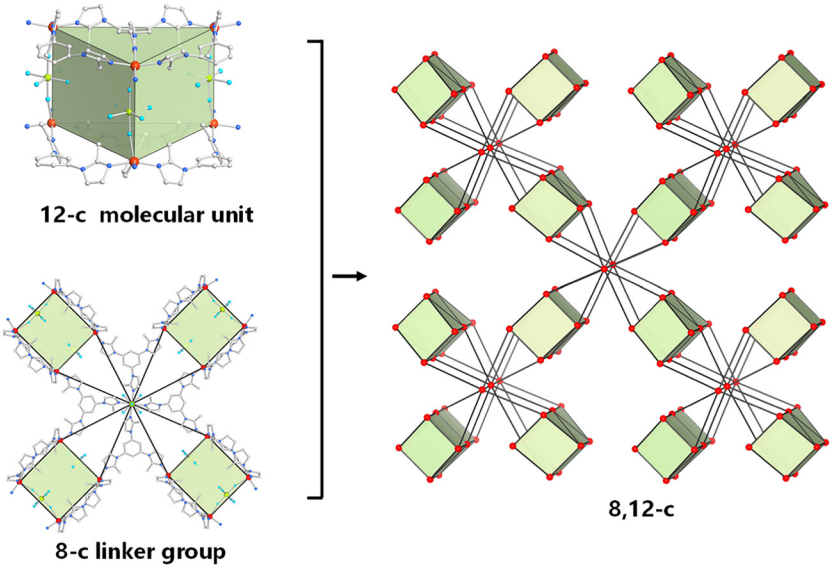

Fig. 6 Schematic representation of the topology of Cu-TMBIB-b: the molecular unit can be considered as a 12-c node, and the linker group can be considered as an 8-c node.

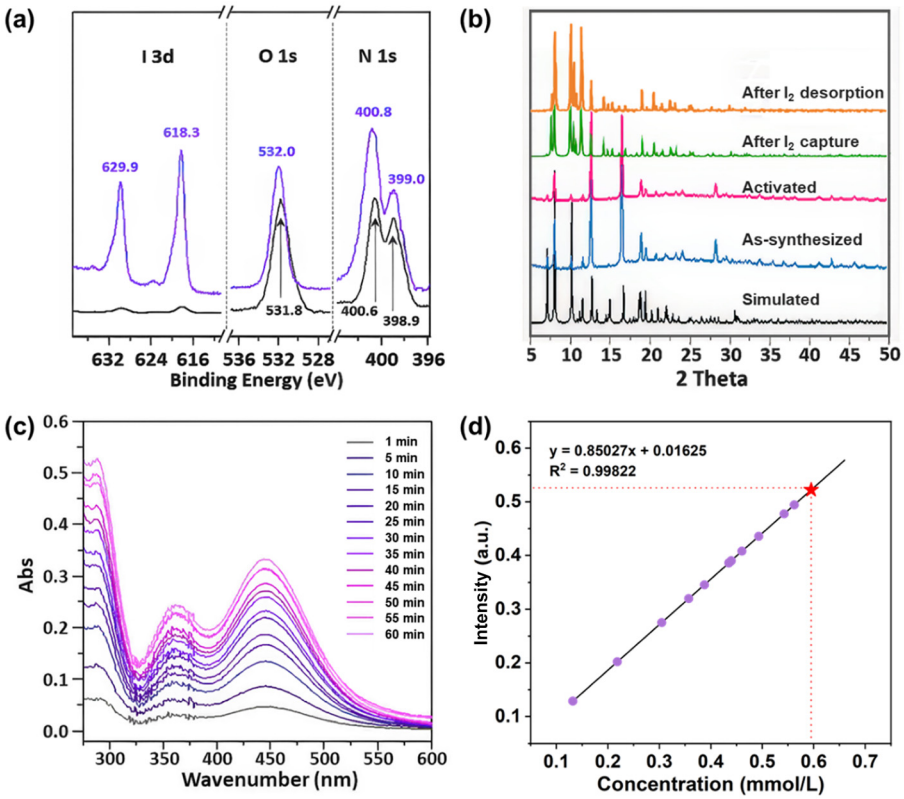

Fig. 7 (a) I 3d, O 1s and N 1s scans of XPS for Cu-TMBIB-a (black line) and I_2@Cu-TMBIB-a (purple line); (b) PXRD patterns of Cu-TMBIB-a (simulated, as-synthesized, after I_2 capture, and after desorption); (c) UV-vis spectra of I_2 releasing from 12.2 mg of I_2@Cu-TMBIB-a in 20 mL of EtOH at different times; and (d) the gradually increasing adsorption intensity with time (purple solid dots) is in good agreement with the standard curve (black solid line), and the red pentagram represents the concentration of the I_2 solution after 60 minutes.

adsorption in molecular form without redox reactions. Pristine Cu-TMBIB-a exhibited a N 1s peak at 398.9 eV corresponding to imidazole N (Fig. S19); after adsorption, the peak upshifted to 400.6 eV, which reflects electron density loss from N atoms and is attributed to charge transfer *via* lone pair donation from N to I_2.[35,36] The O 1s peak of lattice oxygen slightly

 This journal is © The Royal Society of Chemistry 2026

Published on 18 February 2026. Downloaded on 6/17/2026 10:56:24 PM.

shifted from 531.8 eV to 532.0 eV, suggesting weak O–H···I_2 hydrogen bonds stabilizing adsorbed iodine. Iodine adsorption by Cu-TMBIB-a relies on the synergy of pore confinement and weak chemical interactions: size-matching dual pores with diameters of 2.7–2.8 Å trap I_2 *via* van der Waals forces, while N → I charge transfer and O–H···I_2 hydrogen bonds enhance adsorption affinity and ensure reversible desorption. This mechanism explains the high adsorption capacity and recyclability of Cu-TMBIB-a, supporting its potential for practical iodine separation and storage.

4 Conclusions

In this work, two distinct metal–organic frameworks Cu-TMBIB-a and Cu-TMBIB-b were synthesized *via* precise pillar engineering. Using TMBIB as the organic linker and SiF_6^{2-} or TiF_6^{2-} as inorganic pillars, the strategy achieved topological transformation without altering core synthetic parameters. The transformation occurs from the pillar-layered structure of Cu-TMBIB-a with a 3,4,5-c topology to the rare pillar-double-channelled structure of Cu-TMBIB-b with an 8,12-c topology, driven by the geometric and electronic differences of hexafluoride anions. Cu-TMBIB-a exhibited favorable iodine adsorption performance alongside recyclability, with the framework retaining crystallinity during adsorption processes. This study validates pillar engineering as a powerful tool for precise MOF structural regulation, enriches the topological diversity of hexafluoride-pillared MOFs, and underscores the potential of such topology-tailored materials for targeted separation applications.

Author contributions

Shuang Liu: investigation, data curation, writing – original draft and visualization; Chunze Yu: investigation and data curation; Sidan Geng: investigation; Jingui Duan: conceptualization, supervision, review and editing.

Conflicts of interest

There are no conflicts to declare.

Data availability

The data supporting this article have been included as part of the supplementary information (SI). Supplementary information is available. Supporting information includes synthetic procedures of the ligand and crystals, basic characterizations, and detailed structural information. See DOI: https://doi.org/10.1039/d6dt00054a.

CCDC 2521453 and 2521454 contain the supplementary crystallographic data for this paper.[37a,b]

Acknowledgements

This work was financially supported by the National Natural Science Foundation of China (22171135 and 22471235), the Natural Science Foundation of Jiangsu Province (BK20231269), the Outstanding Young Scientist of the Natural Science Foundation of Xinjiang Uygur Autonomous Region (2025D01E06) and the Department of Education of Henan Province (No. 2023GGJS131).

References

1 B. Achenbach, A. Yurdusen, N. Stock, G. Maurin and C. Serre, *Adv. Mater.*, 2025, **37**, 2411359.
2 D. Mukherjee, A. Saha, S. Moni, D. Volkmer and M. C. Das, *J. Am. Chem. Soc.*, 2025, **147**, 5515–5553.
3 Z. Y. Zheng, Q. Y. Lin, Y. Gao, X. F. Ji, J. L. Sessler and H. Y. Wang, *Coord. Chem. Rev.*, 2024, **511**, 215860.
4 I. Senkovska, V. Bon, A. Mosberger, Y. T. Wang and S. Kaskel, *Adv. Mater.*, 2025, **37**, 2414724.
5 Z. S. Han, K. Y. Wang, M. M. Wang and W. Shi, *Acc. Chem. Res.*, 2025, **58**, 625–634.
6 N. P. S. Chauhan, P. Perumal, N. S. Chundawat and S. Jadoun, *Coord. Chem. Rev.*, 2025, **533**, 216536.
7 A. M. Wright, M. T. Kapelewski, S. Marx, O. K. Farha and W. Morris, *Nat. Mater.*, 2025, **24**, 178–187.
8 B. Chettiannan, E. Dhandapani, G. Arumugam, R. Rajendran and M. Selvaraj, *Coord. Chem. Rev.*, 2024, **518**, 216048.
9 S. Duan, L. T. Qian, Y. Zheng, Y. F. Zhu, X. Liu, L. Dong, W. Yan and J. J. Zhang, *Adv. Mater.*, 2024, **36**, 2314120.
10 C. Chen, L. G. Shen, B. Y. Wang, X. C. Lu, S. Raza, J. J. Xu, B. S. Li, H. J. Lin and B. L. Chen, *Chem. Soc. Rev.*, 2025, **54**, 2208–2245.
11 Z. M. Ye, Y. Xie, K. O. Kirlikovali, S. C. Xiang, O. K. Farha and B. L. Chen, *J. Am. Chem. Soc.*, 2025, **147**, 5495–5514.
12 J. H. Wang, F. Y. Kong, B. F. Liu, N. Q. Ren and H. Y. Ren, *Coord. Chem. Rev.*, 2025, **533**, 216534.
13 A. Kondo, S. I. Noro, H. Kajiro and H. Kanoh, *Coord. Chem. Rev.*, 2022, **471**, 214728.
14 A. E. Amooghin, H. Sanaeepur, R. Luque, H. Garcia and B. L. Chen, *Chem. Soc. Rev.*, 2022, **51**, 7427–7508.
15 X. F. Li, H. Bian, W. Q. Huang, B. Y. Yan, X. Y. Wang and B. Zhu, *Coord. Chem. Rev.*, 2022, **470**, 214714.
16 X. Liu, H. Wang, C. Liu, J. W. Chen, Z. Y. Zhou, S. G. Deng and J. Wang, *Chem Bio Eng.*, 2024, **1**, 469–487.
17 S.-i. Noro, R. Kitaura, M. Kondo, S. Kitagawa, T. Ishii, H. Matsuzaka and M. Yamashita, *J. Am. Chem. Soc.*, 2002, **124**, 2568–2583.
18 X. L. Cui, K. J. Chen, H. B. Xing, Q. W. Yang, R. Krishna, Z. B. Bao, H. Wu, W. Zhou, X. L. Dong, Y. Han, B. Li, Q. L. Ren, M. J. Zaworotko and B. L. Chen, *Science*, 2016, **353**, 141–144.
19 S. Noro, S. Kitagawa, M. Kondo and K. Seki, *Angew. Chem., Int. Ed.*, 2000, **39**, 2082–2084.

Published on 18 February 2026. Downloaded on 6/17/2026 10:56:24 PM.

20 S.-i. Noro, D. Tanaka, H. Sakamoto, S. Shimomura, S. Kitagawa, S. Takeda, K. Uemura, H. Kita, T. Akutagawa and T. Nakamura, *Chem. Mater.*, 2009, **21**, 3346–3355.
21 P. Nugent, V. Rhodus, T. Pham, B. Tudor, K. Forrest, L. Wojtas, B. Space and M. Zaworotko, *Chem. Commun.*, 2013, **49**, 1606–1608.
22 A. Cadiau, K. Adil, P. M. Bhatt, Y. Belmabkhout and M. Eddaoudi, *Science*, 2016, **353**, 137–140.
23 Z. Q. Zhang, Q. W. Yang, X. L. Cui, L. F. Yang, Z. B. Bao, Q. L. Ren and H. B. Xing, *Angew. Chem., Int. Ed.*, 2017, **56**, 16282–16287.
24 H. Li, C. P. Liu, C. Chen, Z. Y. Di, D. Q. Yuan, J. D. Pang, W. Wei, M. Y. Wu and M. C. Hong, *Angew. Chem., Int. Ed.*, 2021, **60**, 7547–7552.
25 Q.-L. Qian, X.-W. Gu, J. Pei, H.-M. Wen, H. Wu, W. Zhou, B. Li and G. Qian, *J. Mater. Chem. A*, 2021, **9**, 9248–9255.
26 J. Wang, Y. Zhang, P. Zhang, J. Hu, R.-B. Lin, Q. Deng, Z. Zeng, H. Xing, S. Deng and B. Chen, *J. Am. Chem. Soc.*, 2020, **142**, 9744–9751.
27 Q. Dong, X. Zhang, S. Liu, R.-B. Lin, Y. Guo, Y. Ma, A. Yonezu, R. Krishna, G. Liu, J. Duan, R. Matsuda, W. Jin and B. Chen, *Angew. Chem., Int. Ed.*, 2020, **59**, 22756–22762.
28 S. Liu, Y. H. Huang, J. M. Wan, J. J. Zheng, R. Krishna, Y. Li, K. Ge, J. Tang and J. G. Duan, *Chem. Sci.*, 2024, **15**, 6583–6588.
29 S. Liu, Q. Dong, D. Wang, Y. Wang, H. Wang, Y. Huang, S. Wang, L. Liu and J. Duan, *Inorg. Chem.*, 2019, **58**, 16241–16249.
30 M. Connolly, *J. Appl. Crystallogr.*, 1983, **16**, 548–558.
31 M. O'Keeffe, M. A. Peskov, S. J. Ramsden and O. M. Yaghi, *Acc. Chem. Res.*, 2008, **41**, 1782–1789.
32 L. Y. Wang, H. R. Chen, C. Y. Lou, G. Z. Xiong, Y. J. Jiang, B. L. Chen and Y. B. Zhang, *Angew. Chem., Int. Ed.*, 2025, **64**, e202514808.
33 Y. J. Jiang, L. Y. Wang and Y. B. Zhang, *Chin. J. Struct. Chem.*, 2024, **43**, 100374.
34 X.-T. Liu, Y. Wang and C. Lu, *Chem. Commun.*, 2025, **61**, 17735–17750.
35 J. T. Hughes, D. F. Sava, T. M. Nenoff and A. Navrotsky, *J. Am. Chem. Soc.*, 2013, **135**, 16256–16259.
36 F. Chen, T. Peng, M. Xia, F. Wang and F. Wang, *Nanoscale*, 2026, **18**, 1865–1897.
37 (*a*) CCDC 2521453: Experimental Crystal Structure Determination, 2026, DOI: 10.5517/ccdc.csd.cc2qms6c; (*b*) CCDC 2521454: Experimental Crystal Structure Determination, 2026, DOI: 10.5517/ccdc.csd.cc2qms7d.

 This journal is © The Royal Society of Chemistry 2026